Kinetics and Mechanism of Plasmon-Driven Dehalogenation Reaction of Brominated Purine Nucleobases on Ag and Au

Anushree Dutta[a], *Robin Schürmann*[a], *Sergio Kogikoski Jr.*[a], *Niclas S Mueller*[b], *Stephanie Reich*[b], *Ilko Bald*[a]*

[a]Institute of Chemistry, Physical Chemistry, University of Potsdam, Karl-Liebknecht-Str. 24-25, 14476, Potsdam, Germany.

[b]Department of Physics, Freie Universität Berlin, Arnimallee 14, 14195 Berlin, Germany

Email: *ilko.bald@uni-potsdam.de

Supporting Information

Derivation of the reaction rate law:

$$NP + h\nu \underset{-k_1}{\overset{k_1}{\rightleftharpoons}} e^- + h^+ \qquad \text{(S1)}$$

$$BrNB + e^- \underset{-k_2}{\overset{k_2}{\rightleftharpoons}} BrNB^{*-} \qquad \text{(S2)}$$

$$BrNB^{*-} \xrightarrow{k_3} NB^{\bullet} + Br^- \qquad \text{(S3)}$$

Further we can write,

$$NB^{\bullet} \xrightarrow{k_4} products \qquad (S4)$$

$$NP^*(h^+) + e^- \xrightarrow{k_5} NP \qquad (S5)$$

Equations S4 and S5 are phrased in the most general way and their pathways are discussed in the main text and in more detail in the following discussion. The final equation depends strongly on the specific molecule and reaction conditions and must be explored in more detail in the future.

Considering the above three elementary steps involved in the dehalogenation reaction, the general rate of the plasmon catalysed reaction can be written as below:

Reaction rate of decay of $BrNB$ can be expressed as:

$$\frac{d[BrNB]}{dt} = -k_2\,[BrNB][e^-] + k_{-2}\,[BrNB^{*-}] \qquad (S6)$$

Applying steady state approximation to intermediate $BrNB^{*-}$ (TNI), rate of decay of $BrNB^{*-}$ (TNI) can be written as,

$$\frac{d[BrNB^{*-}]}{dt} = 0$$

Therefore,

$$\frac{d[BrNB^{*-}]}{dt} = k_2\,[BrNB][e^-] - k_{-2}[BrNB^{*-}] - k_3[BrNB^{*-}] = 0$$

or, $$[BrNB^{*-}] = \frac{k_2\,[BrNB][e^-]}{k_{-2}+\,k_3} \qquad (S7)$$

Substituting equation (S7) in equation (S6),

$$\frac{d[BrNB]}{dt} = -\,k_2\,[BrNB][e^-] + \,k_{-2}\,\frac{k_2\,[BrNB][e^-]}{k_{-2}+\,k_3}$$

$$\frac{d[BrNB]}{dt} = \frac{-k_2\,k_3\,[BrNB][e^-]}{k_{-2}+\,k_3} \qquad (S8)$$

$$or,\quad Rate = \frac{d[BrNB]}{dt} = \frac{-k_2\,k_3}{k_{-2}+\,k_3}\quad [BrNB][e^-] \qquad (S9)$$

$$Rate = \frac{d[BrNB]}{dt} = k_{obs}[BrNB][e^-] \qquad (S10)$$

$$where,\ k_{obs} = \frac{-k_2\,k_3}{k_{-2}+\,k_3}$$

Equation S10 represents the general rate equation for the dehalogenation kinetics of brominated purines.

(i) Considering rapid excitation-relaxation process during hot-electrons generation under continuous-wave (CW) illumination[1], the time average local concentration of the hot-electrons $[e^-]$ can be considered to be constant. Therefore, a pseudo first order can be assumed for the dehalogenation rate equation S10 which can be expressed as below:

$$Rate = \frac{d[BrNB]}{dt} = \,k'_{obs}\,[BrNB] \qquad (S11)$$

$$where,\ k'_{obs} = k_{obs}[e^-] = \frac{-k_2\,k_3}{k_{-2}+\,k_3}[e^-] = \frac{-k_2\,k_3\,k_1\,[NP]}{k_{-2}+\,k_3}$$

considering $[e^-] = constant\ and\ [e^-] = k_1\,[NP]$.

(ii) Alternatively, from equation (S11) we can write,

$$k'_{obs} = \frac{-k_2\,k_3\,k_1\,[NP]}{k_{-2}+\,k_3}$$

$$or,\quad \frac{1}{k'_{obs}} = \frac{k_{-2}}{-k_2\,k_3\,k_1\,[NP]} + \frac{k_3}{-k_2\,k_3\,k_1\,[NP]}$$

Alternatively, considering the dissociation of the TNI ($BrNB^{*-}$) to be the fast step, we can write $k_3 \gg k_{-2}$. Therefore,

$$\frac{1}{k'_{obs}} = \frac{1}{-k_1 k_2 [NP]} \quad or, \quad k'_{obs} = -k_1 k_2 [NP]$$

This leads to another simplified pseudo first order equation (S12),

$$Rate = \frac{d[BrNB]}{dt} = k'_{obs} \ [BrNB] \qquad (S12)$$

$$where \ k'_{obs} = -k_1 k_2 [NP]$$

Further, we consider $[BrGua]$ and $[Gua]$to be proportional to the decay and rise in SERS intensity of their ring breathing mode at 693 cm^{-1} and 670 cm^{-1}, respectively. Therefore, the integrated rate expression of equation *S12* can be represented as below:

$$I_{BrNB} = I^{\circ}_{BrAde} e^{-k'_{obs} t} \qquad (S13)$$

Also, $$I_{NB} = I^{\circ}_{BrAde} (1 - e^{-k'_{obs} t}) \qquad (S14)$$

Taking ratio of $\frac{I_{NB}}{I_{BrNB}}$ leads us to the next steps as follows:

$$\frac{I_{NB}}{I_{BrNB}} = \frac{1 - e^{-k'_{obs} t}}{e^{-k'_{obs} t}}$$

or, $$\frac{I_{NB}}{I_{BrNB}} = e^{k'_{obs} t} - 1$$

or, $$e^{k'_{obs} t} = \frac{I_{NB}}{I_{BrNB}} + 1$$

Therefore, equation S12 can be expressed by the relation equation S15,

$$k'_{obs} = \frac{1}{t} \ln(1 + \frac{I_{NB}}{I_{BrNB}}) \qquad (S15)$$

Derivation of integrated first order fractal rate equation

The inhomogeneous distribution of reaction site (substrate) within the illumination zone dominates over the kinetic process (adsorbate) as described in manuscript. This induces a time dependence of the electron transfer in equation S2. The time dependent k'_{obs} is therefore replaced by the relation expressed by equation (S16)[2,3]

$$k_2 = k_f\ t^{-h}\ ,\ 0 \leq h \geq 1\ and\ t \geq 1 \qquad (S16)$$

First order integrated rate equation: We consider first order differential rate law represented by equation (S12) to derive the first order integrated rate equation

$$Rate = \frac{d[BrNB]}{dt} = k'_{obs}\ [BrNB]$$

$$= -k_1\, k_2\, [NP][BrNB]$$

Replacing $k_2 = k_f\ t^{-h}$ in above equation,

$$\frac{d[BrNB]}{dt} = -k_1\, k_f\ t^{-h}[NP][BrNB]$$

$$= k_{f1}\,[BrNB]t^{-h} \qquad (S17)$$

where $k_{f1=}\ k_1\, k_f\ [NP]$ represented first order fractal rate coefficient. Integrating equation (S17) leads to the following first order fractal equation:

$$[BrGua] = [BrGua]_0\ e^{-(k_{f1}\ \frac{t^{1-h}}{1-h})} \qquad 1st\ order\ \ldots \quad (S18)$$

Further, to nullify contribution from background noises arising in heterogeneous systems and to achieve improved goodness of curve fit – ratio of SERS signal intensity of I_{Gua} and I_{BrGua} obtained in Figure 1D (manuscript) have been considered. This leads us to arrive at a new expression representing the pseudo first order (equation S19) fractal rate equation as follows:

$$\frac{I_{Gua}}{I_{BrGua}} = e^{k_{f1}\ \frac{t^{1-h}}{1-h}} - 1 \qquad (S19)$$

Stepwise redox reaction involved in product formation via dehalogenation

The first step involves the generation of hot electrons upon laser illumination followed by transfer of generated primary hot electrons to the lowest unoccupied molecular orbital (LUMO) of adsorbed BrNBs resulting in formation of the TNI BrNB*. The metastable $BrNB^{*-}$ so formed undergoes cleavage of the C–Br bond generating a bromide anion and a nucleobase radical represented by equation (S20-S22)

$$Ag\ \overset{h\nu}{\rightarrow}\ h^+\ + e^- \qquad (S20)$$

$$BrGua \quad + \quad e^- \quad \leftrightharpoons \quad BrGua^{*-} \qquad (S21)$$

$$BrGua^{*-} \quad \rightarrow \quad Gua^{\bullet} \quad + \quad Br^- \qquad (S22)$$

Water oxidation step is as follows: [4]

This is a slow process due to its high oxidation potential of around 1.23 V vs SHE (-5.67 eV) with respect to Fermi energy albeit feasible due to high oxidising power of hot holes.

$$H_2O \quad \rightarrow \quad O_2 \; + \; 4H^+ \; + \; 4e^- \qquad (S23)$$

The $Gua^{\bullet}$ so formed in step $S22$ can undergo reaction following two parallel pathways:

First $Gua^{\bullet}$could translate to form nucleobase Gua consuming an H^+ ion released during the water oxidation step.[5]

$$h^+ \; + e^- \quad \xrightarrow{Gua^{\cdot}} Gua^- \; + \; h^+ \qquad (S24)$$

$$Gua^- \; + \; H^+ \; \rightarrow \; Gua \qquad (S25)$$

and, in a parallel reaction nucleobase radical owing to its high tendency towards oxidation than its neutral counterpart may preferentially undergo oxidation to generate oxo-product of Gua.[6]

$$Gua^{\bullet} + H_2O \quad \rightarrow 8-oxoGua \; + \; e^- \; + \; H^+ \qquad (S26)$$

NOTE: Similar reaction step holds true for BrAde dehalogenation reaction pathway.

Plausible stepwise redox reaction involved in hot hole reduction by bromide anion

The fate of hot holes can be described by a set of redox half reactions at the metal nanoparticle interface. The Br^- by-product participates in favourable one electron transfer reaction to the hole forming photosensitive AgBr on the Ag surface. (Equation S27) Photodisscociation of AgBr further easily regenerates Ag atom (equation S29) and bromide radical to continue the reaction cycle.[7]

$$Ag \; + \; Br^- \; \rightarrow AgBr \; + \; e^- \qquad (S27)$$

(via one step oxidation half reaction)

$$Ag^+/h^+ \; + \; e^- \; \rightarrow \; Ag \qquad (S28)$$

$$AgBr \xrightarrow{h\nu} Ag + Br^{\cdot} \qquad (S29)$$

The $Br^{\cdot}$ generated in Equation S29 can further undergo following side reaction as a part of hole reaction:[8]

$$h^{+} + Br^{-} \rightarrow Br^{\cdot} + e^{-} \qquad (S30)$$

$$Br^{\cdot} + Br^{-} \rightarrow Br_2^{\cdot -} \qquad (S31)$$

$$Br_2^{\cdot -} + Br_2^{\cdot -} \rightarrow Br_2 + 2Br^{-} \qquad (S32)$$

Further, oxidation of nucleobase radical could generate oxo-product of Gua or Ade (equation S33) along with the release of one electron which could be a potential candidate towards hole reduction due to their favourable oxidation potential. [6]

$$NB^{\bullet} + H_2O \rightarrow 8-oxoNB + e^{-} + H^{+} \qquad (S33)$$

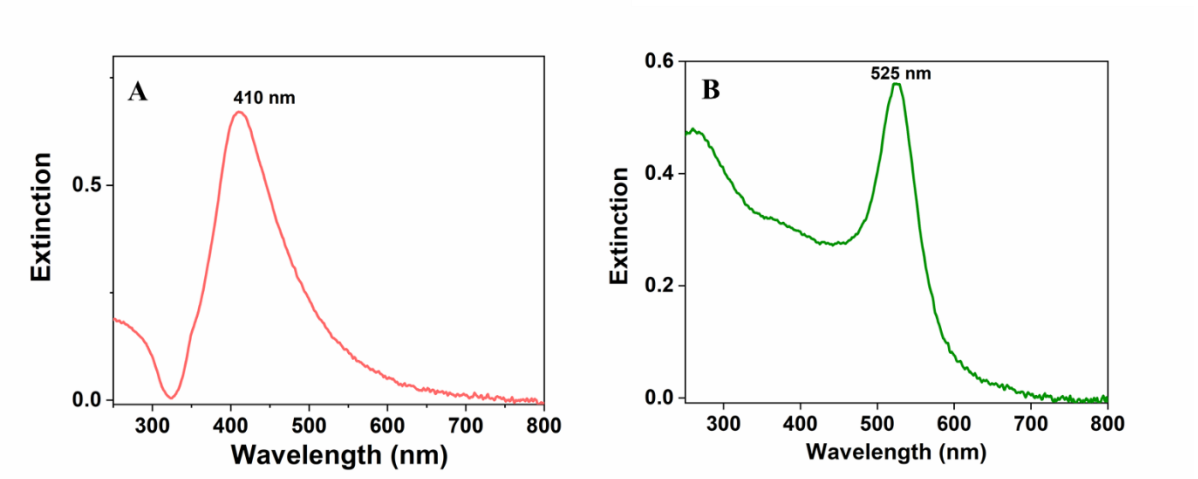

Figure S1. UV-vis spectrum of citrate stabilised (**A**) AgNPs and (**B**) AuNPs dispersion.

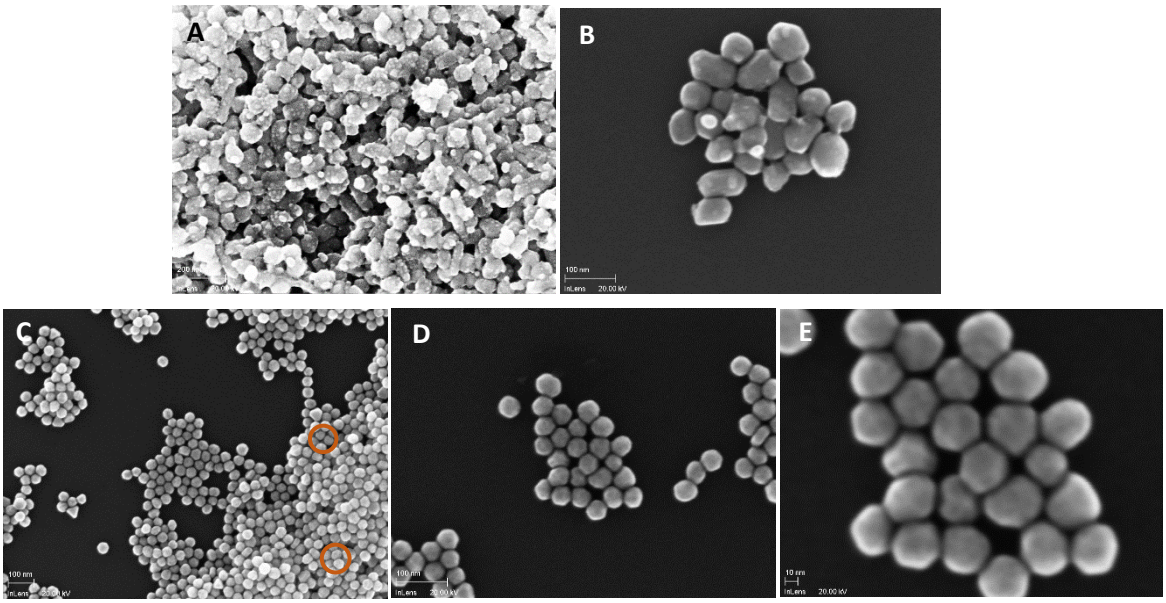

Figure S2. Representative FESEM image of (**A-B**) BrGua coated aggregated AgNPs and (**C-E**) BrGua coated aggregated AuNPs.

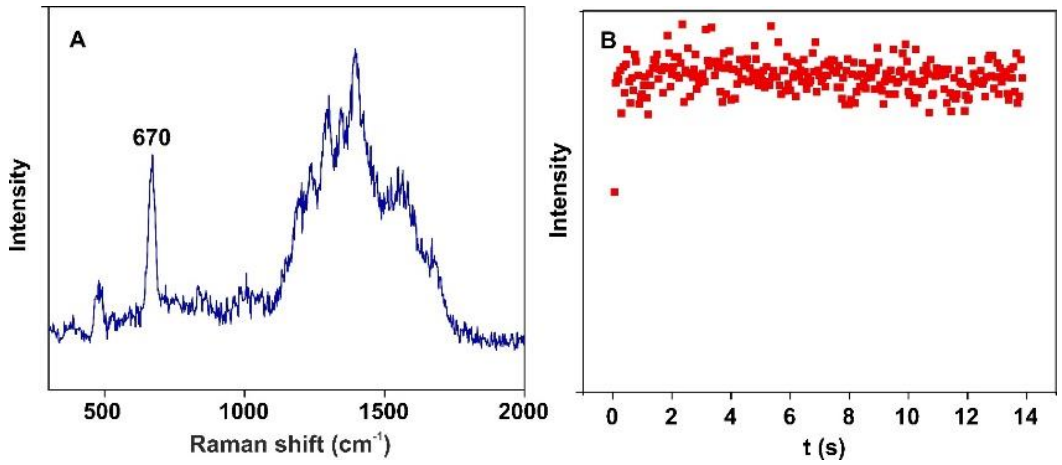

Figure S3. (**A**) SERS spectrum of Gua recorded on aggregated AgNPs under 532 nm CW illumination (laser power: 0.2 mW; data acquisition time: 0.05s; accumulation: 300); (**B**) Intensity of ring breathing mode of Gua at 670 cm^{-1} recorded as a function of illumination time.

Dehalogenation reaction kinetics of BrAde on Ag

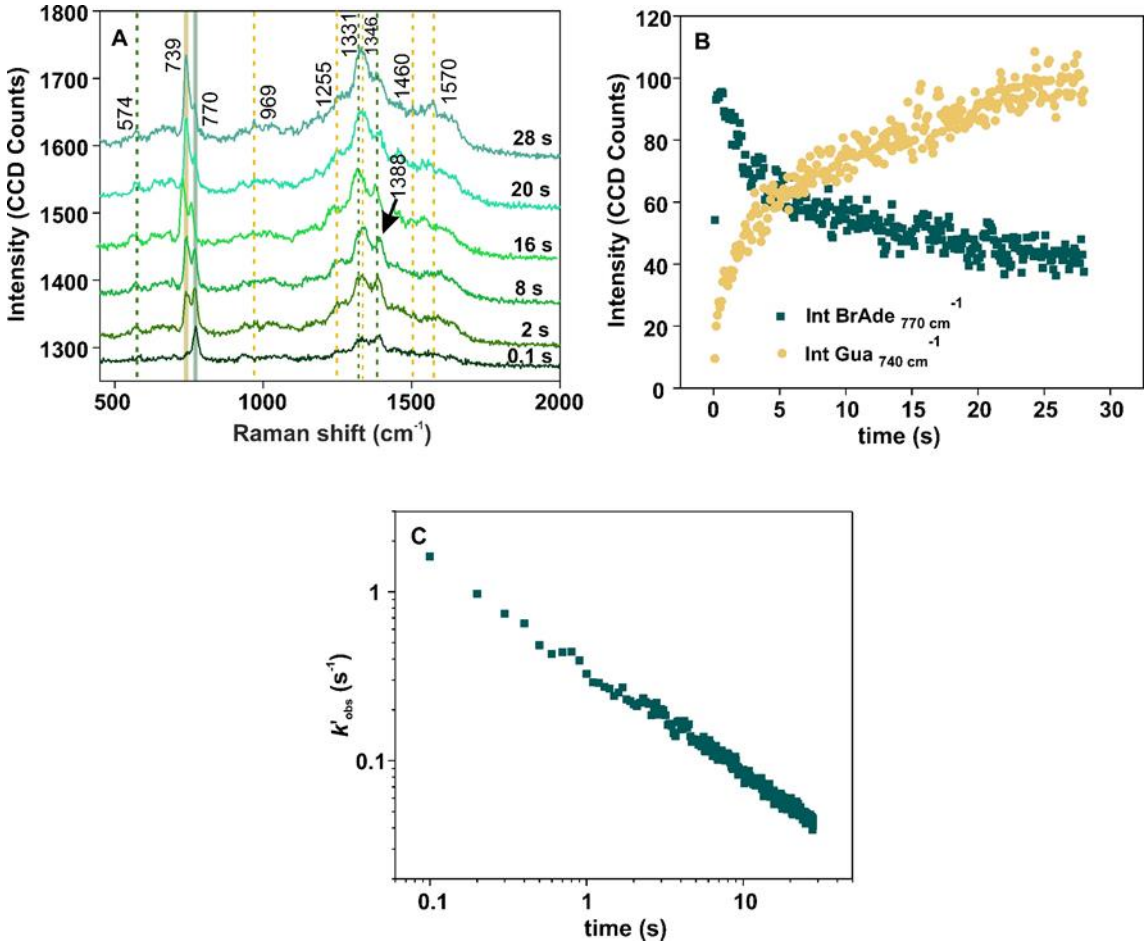

Figure S4. (**A**) SERS spectra recorded during dehalogenation of BrAde on aggregated AgNPs at different illumination time using 532 nm laser source. (laser power: 0.2 mW; data acquisition time: 0.05s; accumulation: 300) Marked bands in green and yellow color correspond to decreasing BrAde and rising Ade vibrational band respectively. (**B**) Plot showing change in SERS intensity of the ring-breathing mode of BrAde at 770 cm^{-1} against that of Ade at 740 cm^{-1} as function of laser illumination time. (**C**) Plot of k'_{obs} obtained (using equation S15) as a function of illumination time.

Time dependent SERS of BrAde measured with 532 nm laser comply with the previously published results, although the illumination parameter considered for kinetic comparisons differs slightly in the present study. Clearly, spectra extracted at t=0.1s showed peak at 770 cm^{-1} and 574 cm^{-1} characteristic to ring breathing mode and $C-Br$ stretching-mode of BrAde respectively along with other vibrational band at 1331 and 1388 cm^{-1} (green dotted lines).[9] The most prominent bands appearing at 770 cm^{-1} in the SERS spectra of BrAde at t=0.1s (Figure S4A) shows a drop in intensity with ongoing illumination time with concomitant rise in peak at 739 cm^{-1} which is assigned to ring breathing mode of Ade.

Appearance of additional new vibrational bands at 969 cm^{-1}, 1346 cm^{-1} 1460 cm^{-1} (C8-H bend) and 1570 cm^{-1} has been assigned to SERS bands of Ade. (Refer ref 9 for vibrational band details and assignments) Interestingly, bands appearing at 1255 cm^{-1} and 1388 cm^{-1} indicated towards the formation of oxo-adduct of Ade.[10]

Similar to BrGua, the kinetics of the BrAde dissociation has been extracted by monitoring the relative change in SERS intensity of ring breathing mode of BrAde at 770 cm^{-1} and rise of ring breathing mode at 739 cm^{-1} of Ade (Figure S4B). The reaction coefficients showed time dependence (Figure S4C using equation S15) similar to what was observed in case of BrGua (Figure S5, SI). This is also in accordance with the previously published results by Schürmann et al. [5]

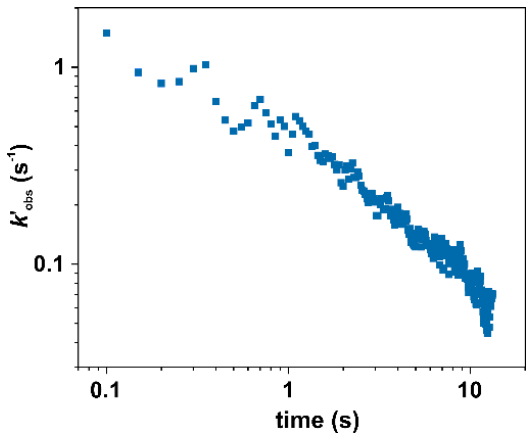

Figure S5. Plot of kinetic rate coefficients (k'_{obs}) obtained from dehalogenation kinetics of BrGua on AgNPs as a function of illumination time using equation S15.

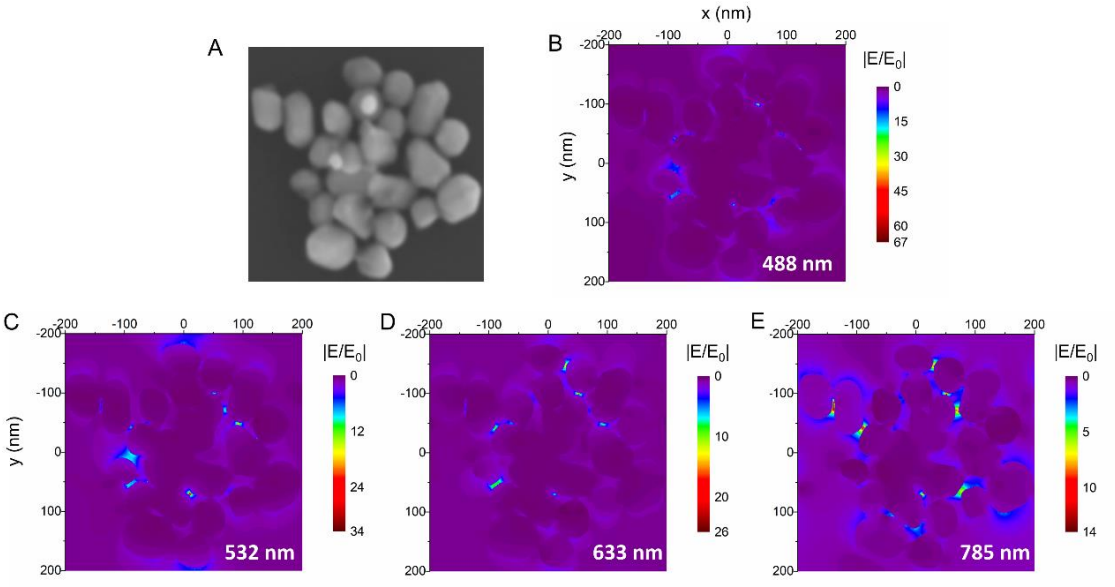

Figure S6. (A) FESEM image from a selected region of BrGua adsorbed Ag aggregates deposited on Si wafer; SERS enhancement values calculated in xy-plane at (B) 488 nm, (C) 532 nm, (D) 632 nm and (E) 785 nm by 3D-FDTD simulation on Ag aggregate shown in FESEM image Figure S6A.

3D-FDTD simulation carried on an exemplary region of BrGua coated Ag aggregates showed maximum field enhancement at 488 nm wavelength corresponding to LSPR region which follows the order: $E_{488} > E_{532} > E_{633} > E_{785}$. A typical example of electric field (EF) enhancement calculated by 3D-FDTD simulation at different laser illumination wavelengths (Figure S6B-E) on a selected region shown in FESEM image (Figure S6A) is included.

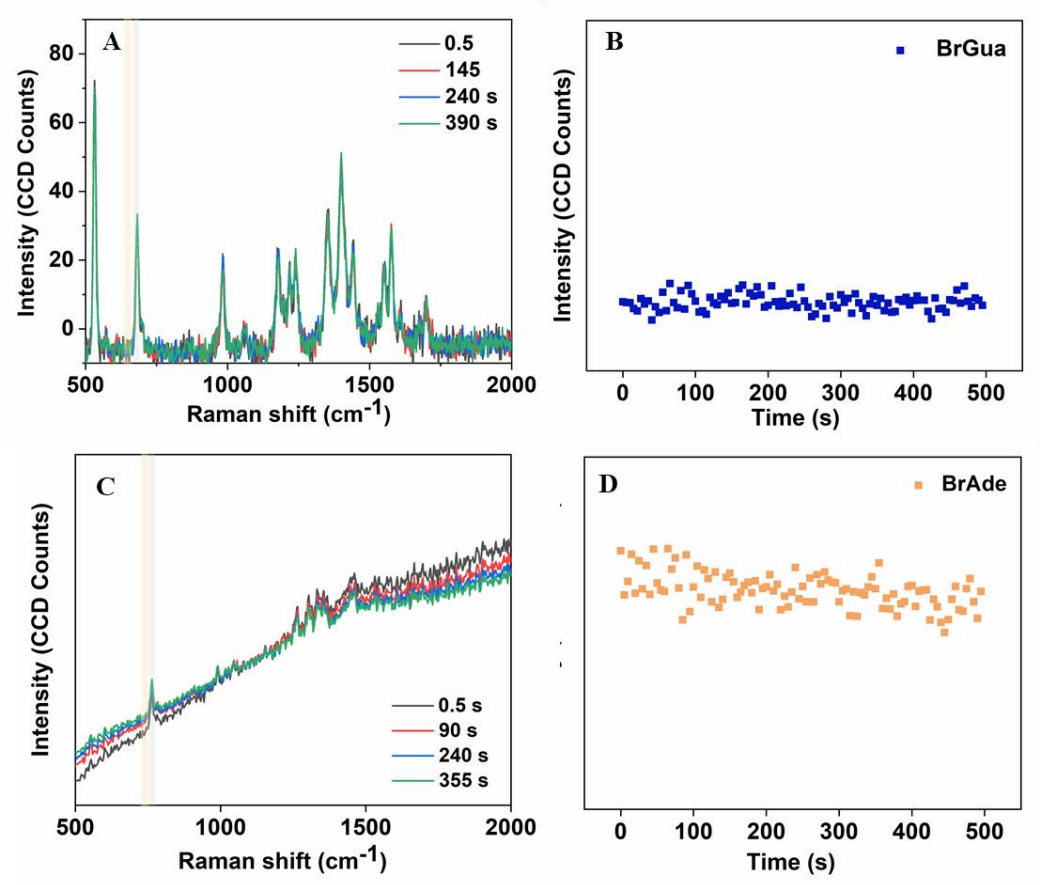

Figure S7. Normal Raman spectra of (**A**) BrGua and (**C**) BrAde recorded with 532 nm laser at different time interval of irradiation. (Objective: 50x; Power: 1mW; acquisition time: 5s). Raman intensity of ring breathing mode of (**B**) BrGua and (**D**) BrAde as function of illumination time. Result showed no cleavage of C-Br bond or decomposition of the bromonucleobases.

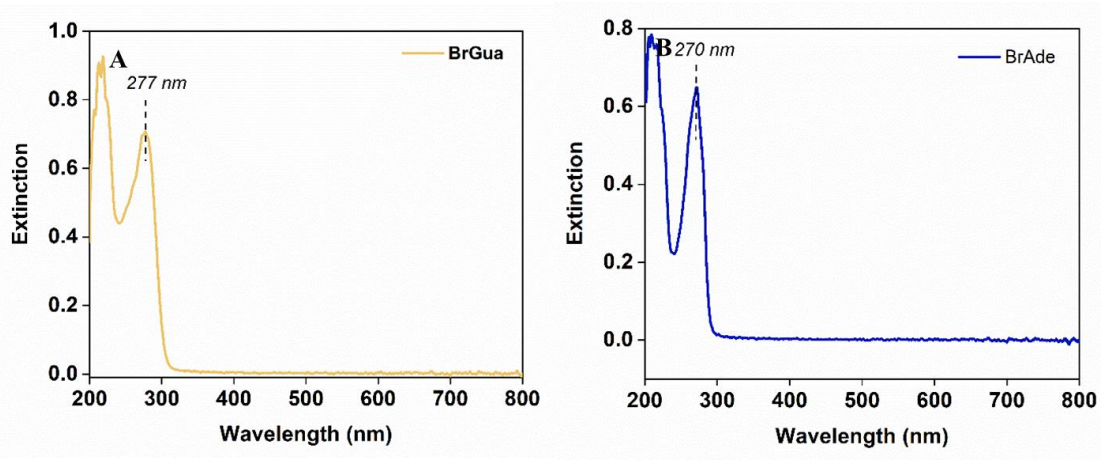

Figure S8. UV-vis spectrum of (A) BrGua and (B) BrAde solution only.

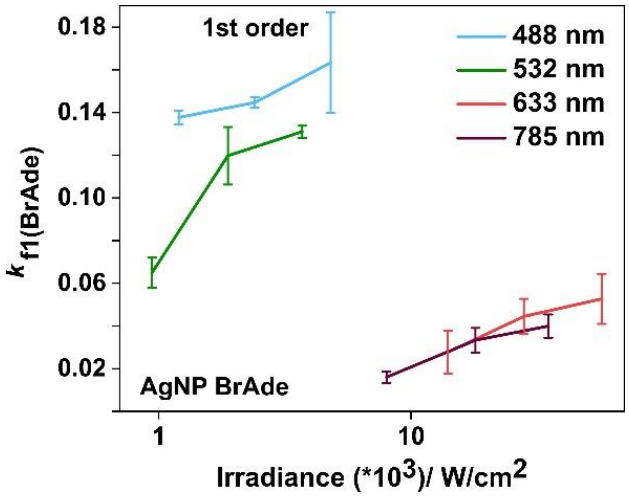

Figure S9. Plot of reaction rate constants as a function of irradiance at different laser wavelength for BrAde coated AgNPs.

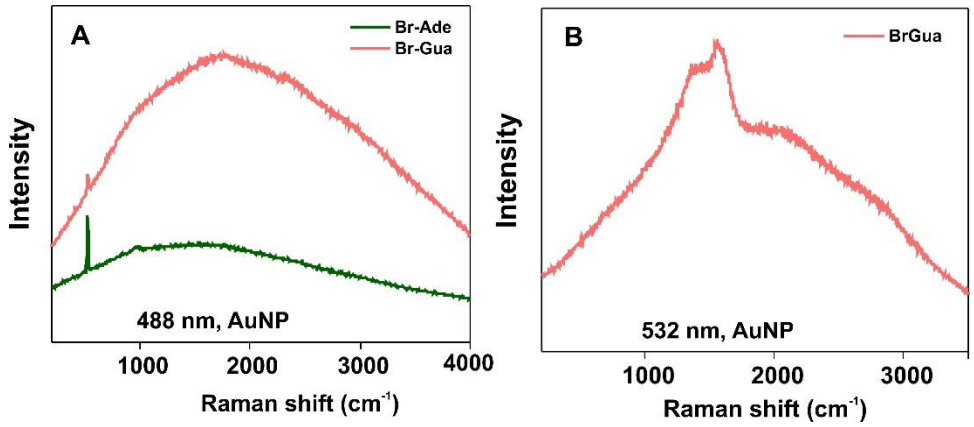

Figure S10. (A) Representative SERS spectra of BrGua and BrAde adsorbed on AuNPs recorded under laser excitation 488 nm (laser power: 1.4 mW; acquisition time: 10 s; accumulation: 10) and (B) that recorded for BrGua using 532 nm laser excitation (laser power: 1.4 mW; acquisition time: 10 s; accumulation: 10).

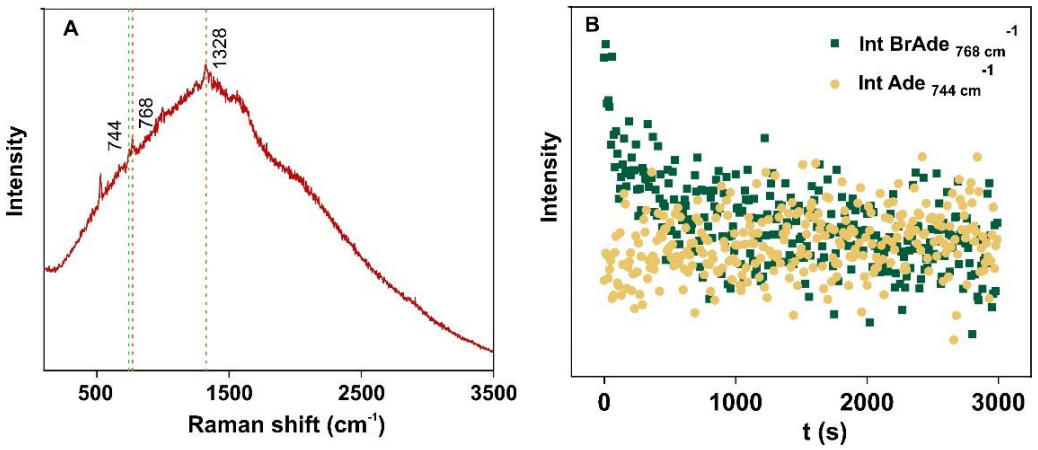

Figure S11. (A) Representative SERS spectra of BrAde adsorbed on AuNPs recorded with 532 nm laser source. (laser power: 6mW; data acquisition time: 10 s; accumulation: 300) and (B) the corresponding change in SERS intensity of ring breathing mode of BrAde and Ade monitored at 768 cm^{-1} and 744 cm^{-1} respectively during the illumination time.

SERS spectra recorded for brominated purines on Au surfaces under laser illumination at 488 nm and 532 nm were dominated by a visible emission background (Figure S10). On the other hand, BrAde showed a very weak signal (of ring stretching vibration) however, with strong emission background when illuminated with the 532 nm laser as shown in Figure S11. This

could be explained by radiative recombination attributed to interband transitions in Au that occur in the range of 2.6-2.8 eV resulting in plasmon damping in addition to off resonance excitation.[11] Figure S11B shows the intensity profile of the ring breathing mode of BrAde (770 cm^{-1}) versus that of Ade (744 cm^{-1}) with time which however does not show discernible changes to deduce reaction kinetics. On the other hand, with 633 nm and 785 nm laser illumination that falls within the SPR wavelength of Au allowed successful measurement of dehalogenation kinetics. The reaction kinetics in case of BrGua and BrAde was drawn in a similar fashion following the relative change in intensity in ring breathing mode of NBs and their brominated analogue as described in the previous sections for Ag. It is to be mentioned that a laser power (6 mW) was required to initiate dehalogenation kinetics of BrGua and BrAde on AuNPs surface which was six times more than that used for the same reaction on AgNPs surfaces for photon energies corresponding to 633 nm and 785 nm.

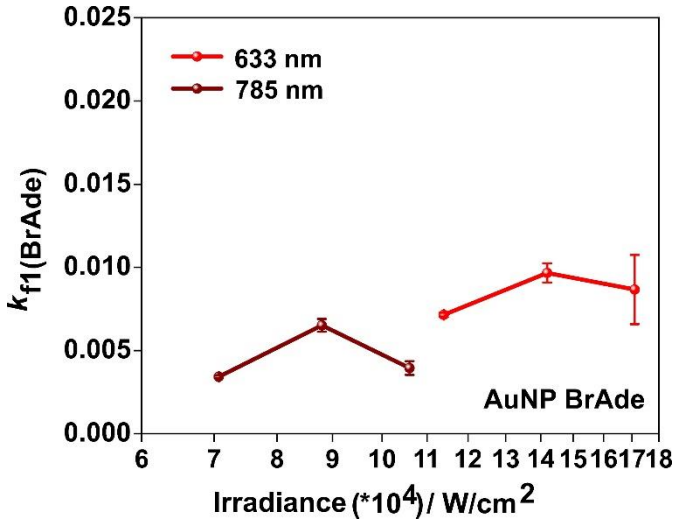

Figure S12. Semi-log plot of reaction rate constant plotted as a function of irradiance at different laser wavelength (X-axis is in log scale) determined for dehalogenation reaction of BrAde on AuNPs. Error bar represents the standard deviation of k_{f1} values from three different independent measurements carried on different reaction spots.

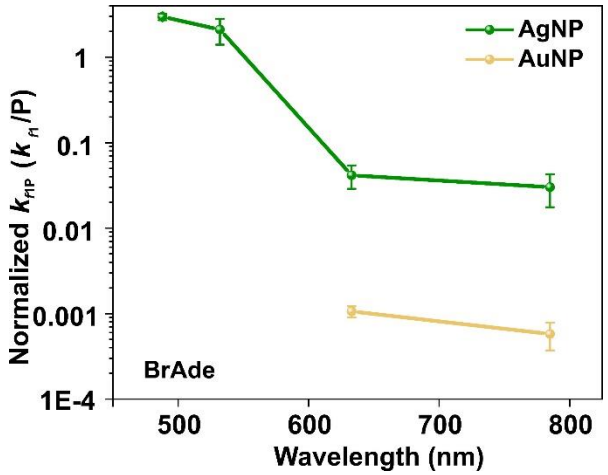

Figure S13. Reaction rate constant (k_{f1}) normalized with respect to lowest laser power (P) in mW and plotted at different laser wavelength for BrAde adsorbed on AgNPs (green) and AuNPs (yellow). Error bar represents the standard deviation of $k_{f1/P}$ values from three different independent measurements. (Y-axis is in log scale)

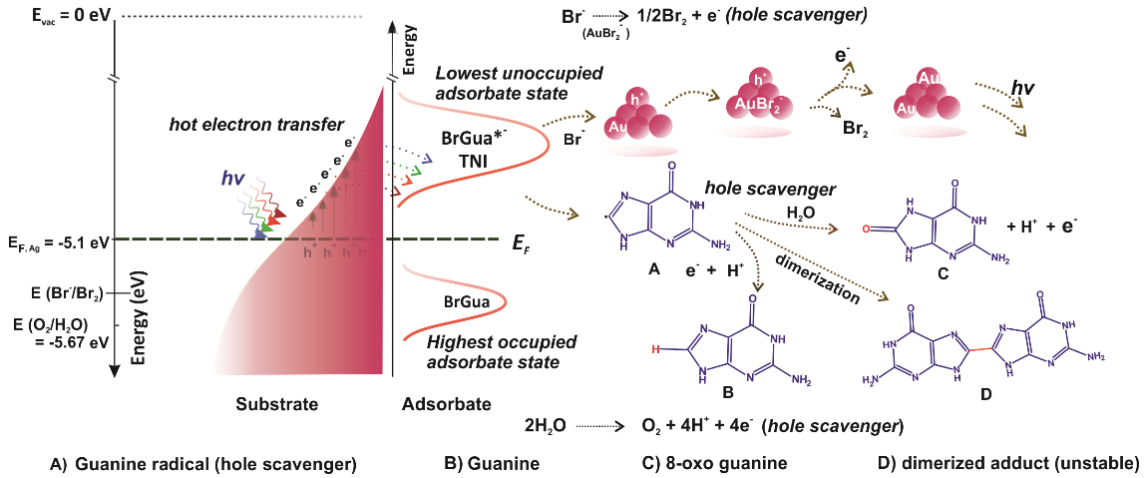

Scheme S1. Schematic representation of the overall plasmon induced dehalogenation process and plausible pathway of hot hole reaction and fate of nucleobase radical (taking the example of BrGua) on Au surface. (energy levels shows absolute electrochemical energies, E (eV) with respect to the vacuum level)

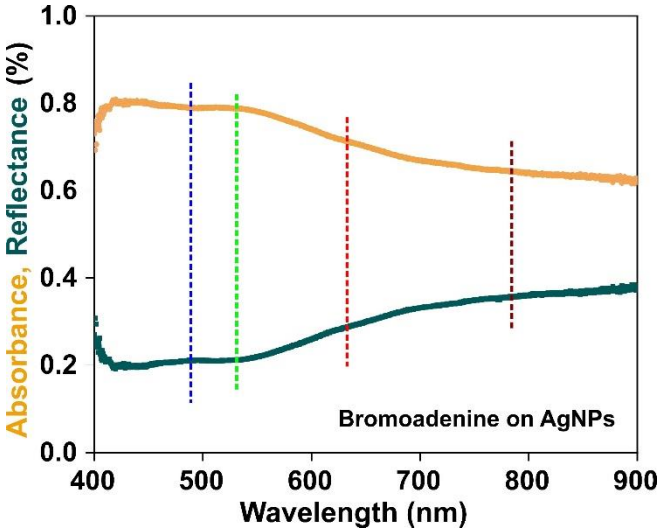

Figure S14. Absorbance and corresponding reflectance spectra recorded for BrAde coated AgNPs. **Figure S15B** shows the microscopic image of AgNPs where the present spectral data is recorded. High absorbance at 488 nm spectral regions explains the highest reaction coefficient observed at 488 nm laser excitation while that recorded with 785 nm laser illumination being the minimum.

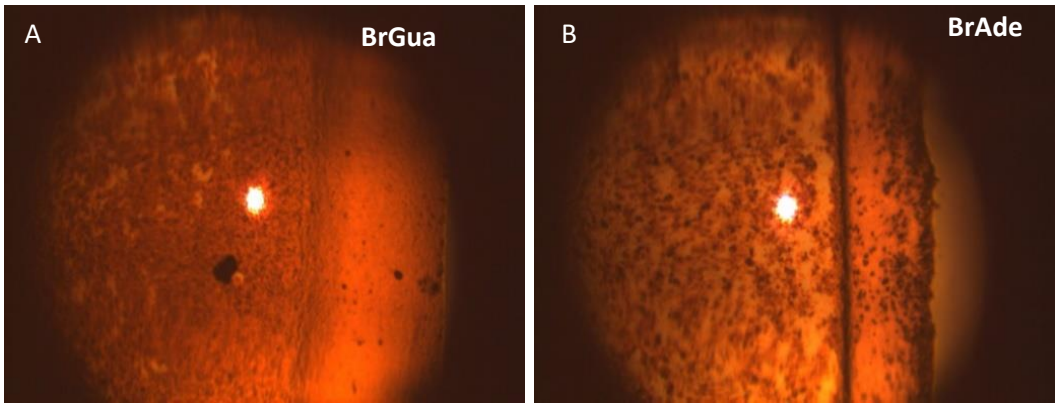

Figure S15. Microscopic images of (**A**) BrGua and (**B**) BrAde coated aggregates of AgNPs with bright spot showing the regions where absorbance and reflectance spectra were recorded.

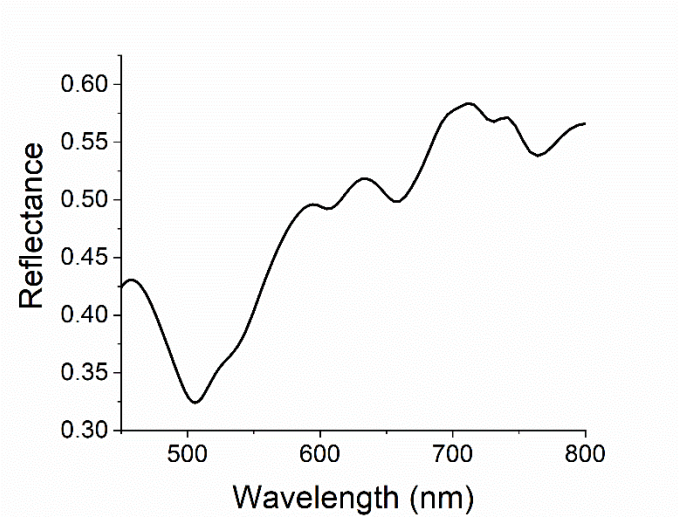

Figure S16. 3D-FDTD simulated reflectance spectra obtained from the region shown in FESEM image in **Figure S6A**.

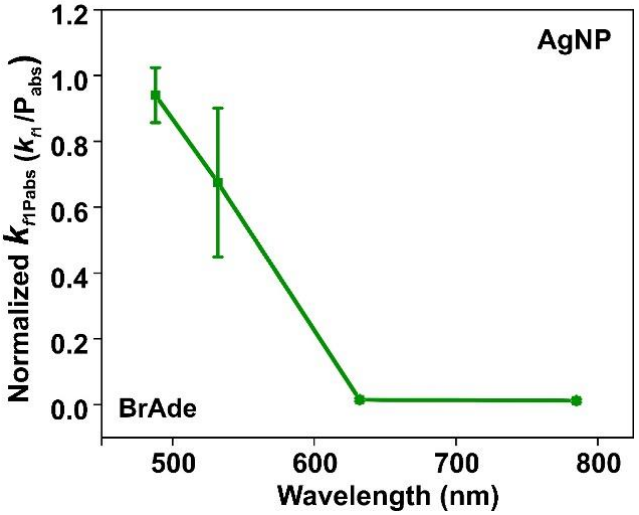

Figure S17. Rate coefficients (k_{f1}) normalized with respect to absorbed laser power (P_{abs} in mW) expressed by $k_{f1P_{abs}}$ ($k_{f1P_{abs}} = k_{f1}/P_{abs}$) plotted at different laser wavelength for BrAde coated AgNPs. P_{abs} = Incident power×Absorbance. The absorbance of the substrate used for the normalization has been determined from micro-absorbance measurement in **Figure S14**.

Plausible explanation for observed reactivity of BrGua and BrAde on Ag and Au surfaces:

The apparent binding affinity of nucleobases for Au follows the order: Gua>Ade>Cyt>Thy (based on heat of desorption, $\triangle H_{des}$).[12] Further to be mentioned that the Gua and BrGua, owing to their insolubility in water were studied in slightly different condition (basic). Therefore, relatively high hydroxide ion concentration in the dispersion could additionally induce enolisation of C=O functional moiety thereby, driving stronger interaction of BrGua with AuNPs than BrAde. Studies indicate change in surface state energy upon adsorbate binding, which would have influence on the reactivity of the respective adsorbates. For example, binding mode of Gua on AuNPs studied by DFT reveals surface quantum trapping effect resulting in valence band shift towards the Fermi level.[13]Therefore due to this effect, electron donation from lone pair orbital of N to unoccupied orbital of Au is accompanied by π or σ-back donation from polarized Au valence charges contributing towards strong complex with Gua.[14] Such valence band shift upon Gua binding on Au could therefore lead to faster reaction pathway. Therefore, considering the fact and binding affinity mentioned, relatively higher reaction rate of BrGua on Au NPs surface over BrAde could be speculated.

Further, the electrophilic nature of the BrNBs follows the order: $\mathrm{BrGua} \leq \mathrm{BrAde} < \mathrm{BrCyt} < \mathrm{BrUra}$ (supported by adiabatic electron affinity (AEA) values[14] calculated by Chomicz et al. indicating towards higher reaction rate of BrAde over BrGua towards dehalogenation via TNI formation. Additionally, adsorption study of adenine on (111) surface of Ag showed an upward energetic shift of density of states native to adenine only.[15] Therefore, considering the surface state shift that occurs on adsorbate binding and strength of the nucleobases binding on AgNPs: $Ade > Ura > Thy > Cyt \geq Gua$ (determined by colorimetric method)[16] higher reactivity of BrAde on AgNPs surface than BrGua could be interpreted. We herein present a plausible explanation to support the observed reactivity of BrGua and BrAde adsorbed on AuNPs and AgNPs surface and vice versa, without taking into account the substituent effects in the bromo-analogues of Gua and Ade that might affect the above said binding affinity. [17]

An additional argument which can be placed is – different nucleobases and their derivatives induces aggregation among NPs upon adsorption, the extent of which depends upon their binding affinity with the NP surface.[16,18] The varying strength of the nucleobases

to interact with the surface of NPs (as discussed above) arises due to the presence of different functional moieties and their ability to display different possible nonspecific chemical interactions inducing aggregation in the system. This results in the generation of local hot-spots among the aggregates where the electric field enhancement is highest compared to the rest of the metallic surface. As the local reaction rate correlates with the electromagnetic enhancement at the hot-spot,[19] therefore higher number of hot-spots generated during aggregation based on interaction of nucleobases with plasmonic substrate might play a deciding role for the differences observed in the reaction kinetic rate.[5,20]

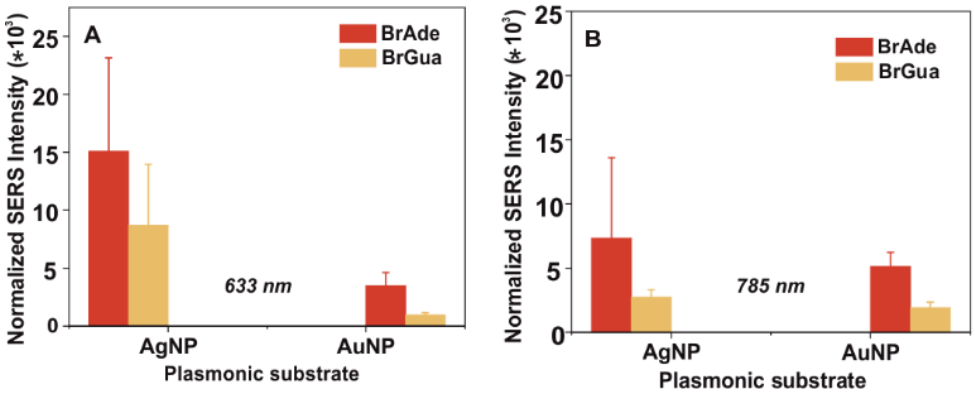

Figure S18. Histogram plot showing the comparison of normalized SERS intensity (normalized with respect to laser power) of BrAde and BrGua on AgNPs and AuNPs under (A) 633 nm and (B) 785 nm laser excitation.

References

(1) Zhang, Z.; Zhang, C.; Zheng, H.; Xu, H. Plasmon-Driven Catalysis on Molecules and Nanomaterials. *Acc. Chem. Res.* **2019**, *52*, 2506–2515.

(2) Kopelman, R. Fractal Reaction Kinetics. *Science* **1988**, *241*, 1620–1626.

(3) Sieland, F.; Schneider, J.; Bahnemann, D. W. Fractal Charge Carrier Kinetics in TiO_2. *J. Phys. Chem. C* **2017**, *121*, 24282–24291.

(4) Kim, Y.; Smith, J. G.; Jain, P. K. Harvesting Multiple Electron-Hole Pairs Generated through Plasmonic Excitation of Au Nanoparticles. *Nat. Chem.* **2018**, *10*, 763–769.

(5) Schürmann, R.; Bald, I. Real-Time Monitoring of Plasmon Induced Dissociative Electron Transfer to the Potential DNA Radiosensitizer 8-Bromoadenine. *Nanoscale*

2017, *9*, 1951–1955.

(6) Ibañez, D.; Santidrian, A.; Heras, A.; Kalbáč, M.; Colina, A. Study of Adenine and Guanine Oxidation Mechanism by Surface-Enhanced Raman Spectroelectrochemistry. *J. Phys. Chem. C* **2015**, *119*, 8191–8198.

(7) Xie, W.; Schlücker, S. Hot Electron-Induced Reduction of Small Molecules on Photorecycling Metal Surfaces. *Nat. Commun.* **2015**, *6*, 7570.

(8) Tsai, K. Y. Da; Chang, I. J. Photocatalytic Oxidation of Bromide to Bromine. *Inorg. Chem.* **2017**, *56*, 693–696.

(9) Dutta, A.; Schürmann, R.; Bald, I. Plasmon Mediated Decomposition of Brominated Nucleobases on Silver Nanoparticles – A Surface Enhanced Raman Scattering (SERS) Study. *Eur. Phys. J. D* **2020**, *74*, 1–9.

(10) Ibañez, D.; Santidrian, A.; Heras, A.; Kalbáč, M.; Colina, A. Study of Adenine and Guanine Oxidation Mechanism by Surface- Enhanced Raman Spectroelectrochemistry. J. *Phys. Chem. C* **2015**, *119*, 8191−8198.

(11) Zhang, X.; Huang, C.; Wang, M.; Huang, P.; He, X.; Wei, Z. Transient Localized Surface Plasmon Induced by Femtosecond Interband Excitation in Gold Nanoparticles. *Sci. Rep.* **2018**, *8* , 1–7.

(12) Demers, L. M.; Östblom, M.; Zhang, H.; Jang, N. H.; Liedberg, B.; Mirkin, C. A. Thermal Desorption Behavior and Binding Properties of DNA Bases and Nucleosides on Gold. *J. Am. Chem. Soc.* **2002**, *124* , 11248–11249.

(13) Zhang, X.; Sun, C. Q.; Hirao, H. Guanine Binding to Gold Nanoparticles through Nonbonding Interactions. *Phys. Chem. Chem. Phys.* **2013**, *15*, 19284–19292.

(14) Chomicz, L.; Rak, J.; Storoniak, P. Electron-Induced Elimination of the Bromide Anion from Brominated Nucleobases. A Computational Study. *J. Phys. Chem. B* **2012**, *116*, 5612–5619.

(15) Andrews, K. M.; Pearl, T. P. Modification of Ag(111) Surface Electronic Structure via Weak Molecular Adsorption of Adenine Measured with Low Temperature Scanning Tunneling Microscopy and Spectroscopy. *J. Chem. Phys.* **2010**, *132*, 214701(1-7).

(16) Yu, L.; Li, N. Binding Strength of Nucleobases and Nucleosides on Silver Nanoparticles Probed by a Colorimetric Method. *Langmuir* **2016**, *32*, 5510−5518

(17) Szatylowicz, H.; Jezuita, A.; Marek, P. H.; Krygowski, T. M. Substituent Effects on the Stability of the Four Most Stable Tautomers of Adenine and Purine. *RSC Adv.* **2019**, *9*, 31343–31356.

(18) Schürmann, R.; Bald, I. Decomposition of DNA Nucleobases by Laser Irradiation of Gold Nanoparticles Monitored by Surface-Enhanced Raman Scattering. *J. Phys. Chem. C* **2016**, *120*, 3001–3009.

(19) Cortés, E.; Xie, W.; Cambiasso, J.; Jermyn, A. S.; Sundararaman, R.; Narang, P.; Schlücker, S.; Maier, S. A. Plasmonic Hot Electron Transport Drives Nano-Localized Chemistry. *Nat. Commun.* **2017**, *8*, 1–10.

(20) Gargiulo, J.; Berté, R.; Li, Y.; Maier, S. A.; Cortés, E. From Optical to Chemical Hot Spots in Plasmonics. *Acc. Chem. Res.* **2019**, *52*, 2525–2535.